Carbohydrate Polymers 87 (2012) 1919–1924

Contents lists available at SciVerse ScienceDirect

Carbohydrate Polymers

journal homepage: www.elsevier.com/locate/carbpol

Characterization of magnetic guar gum-grafted carbon nanotubes and the adsorption of the dyes

Li Yan[a], Peter R. Chang[b], Pengwu Zheng[a,*], Xiaofei Ma[c]

[a] School of Pharmacy, Jiangxi Science and Technology Normal University, Nanchang, Jiangxi 330013, China
[b] Bioproducts and Bioprocesses National Science Program, Agriculture and Agri-Food Canada, 107 Science Place, Saskatoon, SK S7N 0X2, Canada
[c] Chemistry Department, School of Science, Tianjin University, Tianjin 300072, China

ARTICLE INFO

Article history:
Received 1 September 2011
Received in revised form
23 September 2011
Accepted 28 September 2011
Available online 4 October 2011

Keywords:
Nanocomposites
Guar gum
Multiwall carbon nanotube
Magnetic separation
Dye

ABSTRACT

The hydrophobicity of carbon nanotubes (CNTs) limits their extensive application. The hydrophilicity and biocompatibility of CNTs can be improved by modifying them with biopolymers. As a natural biopolymer, guar gum (GG) was covalently grafted on the surfaces of multiwall carbon nanotube (MWCNT) to obtain GG–MWCNT composite. Then iron oxide nanoparticles were synthesized on the GG–MWCNT to prepare the magnetic GG–MWCNT–Fe_3O_4. The obtained nanocomposites were characterized by Fourier transform infrared spectroscopy, thermogravimetric analysis, transmission electron microscopy, ultraviolet–visible (UV–vis) spectroscopy and X-ray diffraction. GG–MWCNT was composed of about 21.6 wt% GG components, which enhanced the dispersion of GG–MWCNT in aqueous solution and also acted as a template for growth of iron oxide nanoparticles. GG–MWCNT–Fe_3O_4 exhibited superparamagnetic with a saturation magnetization (13.3 emu g^{-1}), and good adsorption on neutral red and methylene blue. GG–MWCNT–Fe_3O_4 could be easily separated from the aqueous solution in a magnetic field.

1. Introduction

Many industries (such as dyestuffs, textile, paper and plastics) use dyes, many of which are toxic and even carcinogenic and this poses a serious hazard to aquatic living organisms (Crini, 2006). Carbon nanotubes (CNTs) are considered to be promising adsorbents due to its unique chemical structure and intriguing physical properties. Numerous studies have demonstrated their potential in the removal of metallic ions and organic compounds from aqueous solutions (Wang, Yang, & Hsieh, 2011). However, a large number of CNTs applications are hampered by the hydrophobic properties of CNTs. It is desirable to modify the hydration properties of the surfaces of CNTs so that they become hydrophilic.

Many biopolymers have been used to modify the CNTs by covalent modification or non-covalent functionalization because of their hydrophilicity (Lin et al., 2004). Chitosan was grafted onto MWCNTs by covalent modification of MWCNT with completely deacetylated chitosan (Wu et al., 2007). The starch/carboxylated multiwall carbon nanotube composite (CCNT–starch) was prepared by covalently grafting starch onto the surfaces of CCNT, and the dispersion of CCNT–starch in water was improved (Yan, Chang, & Zheng, 2011). Ke (2010) covalently functionalized the MWNTs with the cellulose acetate using 2, 4, 6-trichloro-1, 3, 5-triazine, as intermediated functional groups. Amylose can form single helix in solutions, which may act as a host molecule to complex hydrophobic CNTs by non-covalent hydrophobic interactions (Fu, Meng, Lu, Zhang, & Gao, 2007). Amylose/single-walled carbon nanotubes (SWCNTs) composites were prepared in aqueous solutions and deposited as films (Bonnet, Albertini, Bizot, Bernard, & Chauvet, 2007). SWCNTs were treated with a cellulose solution in the ionic liquid 1-butyl-3-methylimidazolium bromide to obtain SWCNTs wrapped with cellulose, which could be dispersed in water, forming a stable solution with excellent biocompatibility (Li, Meng, Zhang, Fu, & Lu, 2009). A method was described for the wet spinning of alginate fibers with a loading of SWCNTs as high as 23 wt%. Electrostatic assembling of polyelectrolytes and nanotubes coated with sodium dodecyl sulfate was exploited by using calcium as a cross-linking agent (Sa & Kornev, 2011).

Guar gum is a natural hydrophilic polysaccharide obtained from the endosperm of the guar plant, which has been extensively used in various industrial applications. It is an inherently biocompatible, biodegradable and non-toxic nature biopolymer. In this work, the grafting of GG onto the surface of CNTs was firstly prepared to expectantly improve the hydrophilicity of CNTs and possess excellent properties of CNTs such as the efficient adsorption for removing many kinds of organic and inorganic contaminants (Long & Yang,

* Corresponding author. Tel.: +86 791 3805385; fax: +86 791 3805385.
E-mail address: zhengpw@126.com (P. Zheng).

0144-8617/$ – see front matter.
doi:10.1016/j.carbpol.2011.09.086

2001; Yan et al., 2011). The magnetic separation technology (Gong et al., 2009; Xie, Qian, Wu, & Ma, 2011) was also used. Iron oxide nanoparticles were synthesized on the GG–MWCNT to obtain the magnetic GG–MWCNT–Fe_3O_4, which made the separation process conveniently.

2. Experimental

2.1. Materials

The purified MWCNTs were provided by the Department of Chemical Engineering, Tsinghua University, and synthesized from ethylene and propylene gas via catalytic (Fe/Al_2O_3 as the catalyst) chemical vapor deposition (Wang, Wei, Luo, Yu, & Gu, 2002). GG was provided by Jingkun Chemistry Company, Jiangsu, China. Neutral red (NR) and methylene blue (MB) were provided by Tianjin Benchmark Chemical Reagent Co., Ltd. All other reagents were of analytical grade and used as received, purchased from Tianjin Chemical Reagent Factory (Tianjin, China).

2.2. Preparation of GG–MWCNT and GG–MWCNT–Fe_3O_4

The crude MWCNT were treated with nitric acid (120 mL) and stirred for 14 h at 120 °C, then it was separated by filtration, washed with twice-distilled water to the neutral and dried, and finally the oxidized MWCNT (MWCNT–COOH) was formed. The suspension of MWCNT–COOH (0.7 g) was stirred in a solution of thionyl chloride (30 mL) and DMF (1 mL) for 24 h at 70 °C, then it was filtrated and dried in vacuum for 3 h. For the preparation of GG–MWCNT, GG (0.2 g) was added to DMF (30 mL) and pyridine (1 mL) solution and stirred for 24 h at 110 °C. The product was collected by filtration, sonicated with DMAC/LiCl at room temperature, then washed with distilled water and dried. Finally the product was triturated to get a fluffy solid.

The GG–MWCNT–Fe_3O_4 were prepared from a suspension of 0.25 g GG–MWCNT in the 100 mL solution of 0.745 g $FeCl_3{\cdot}6H_2O$ and 0.3825 g $FeSO_4{\cdot}7H_2O$ at 60 °C under N_2 atmosphere. $NH_3{\cdot}H_2O$ solution (10 mL, 8 mol L^{-1}) was added into the solution and the pH of the final mixtures was controlled at the range of 10–11. The mixture solution were stirred for 4 h at 60 °C and then washed to neutral with distilled water. Finally, the obtained composite was dried at about 80 °C.

2.3. Fourier transform infrared spectroscopy (FTIR)

FTIR spectra of GG, MWCNT, GG–MWCNT and GG–MWCNT–Fe_3O_4 were recorded on a BIO-RAD FTS3000 IR Spectrometer.

2.4. Transmission electron microscopy (TEM)

The microstructure of GG–MWCNT and GG–MWCNT–Fe_3O_4 was observed by transmission electron microscopy (TEM). Drops of samples aqueous suspensions were delivered onto the copper grid and dried in air. The samples were analyzed by using a TEM JEM-1200EX.

2.5. Thermogravimetric analysis (TGA)

TGA of GG and GG–MWCNT were measured using a ZTY-ZP type thermal analyzer. Sample weights varied from 10 to 15 mg and which were heated from room temperature to 600 °C at a heating rate of 15 °C min^{-1} in the nitrogen atmosphere.

2.6. The UV–vis spectroscopy

The UV–vis spectra of MWCNT and GG–MWCNT with different concentrations in distilled water were tested. The spectra showed featureless absorption in the 300–800 nm regions. The samples were recorded by using a UV–vis spectrophotometer model U-1800, Hitachi Company.

2.7. XRD

GG–MWCNT–Fe_3O_4 powders were placed in a sample holder for X-ray diffraction (XRD). XRD patterns were recorded in reflection mode in the angular range of 10–80° (2θ), at ambient temperature, by Rigaku D/max 2500v/pc (Japan) operated at a CuKα wavelength of 1.542 Å.

2.8. The magnetic properties of GG–MWCNT–Fe_3O_4

The magnetic properties of GG–MWCNT–Fe_3O_4 was measured on a vibrating sample magnetometer (LDJ 9600-1, LDJ Electronics Inc., U.S.A.) with the magnetic field set at up to 1.0 T.

2.9. Adsorption experiments

The adsorption experiments were conducted individually for MB and NR dyes. The glass bottles contained 10 mL 1 g L^{-1} of GG–MWCNT–Fe_3O_4 and the dyes (0.1 mmol L^{-1}) solution, which were placed in a slow-moving platform shaker and aliquots solution. The solutions were taken out at different time intervals during the adsorption. The GG–MWCNT–Fe_3O_4 was separated from solution by exposing to a magnet. The dye (MB or NR) concentrations in the solution were analyzed by UV–vis spectrometry and relative dye adsorption versus reaction time was determined. The adsorbed amount of dyes at time t (q_t, mg g^{-1}) was calculated by using Eq. (1) (Chatterjee, Chatterjee, Lim, & Woo, 2011).

$$q_t = \frac{(C_0 - C_t)V}{W} \quad (1)$$

where C_0 and C_t (mg mL^{-1}) are the concentrations of dye solution at initial and t time, respectively; V (mL) is the volume of solution and W (g) is the weight of GG–MWCNT–Fe_3O_4.

Adsorption isotherms were studied by adding 10 mL 1 g L^{-1} of GG–MWCNT–Fe_3O_4 and dye concentrations from 0.05 to 0.6 mmol L^{-1}. After the suspensions were shaken for 6 h, the GG–MWCNT–Fe_3O_4 was separated from solution by exposing to a magnet.

3. Results and discussion

3.1. Characterization of GG–MWCNT

Fig. 1a shows FTIR spectra of GG, MWCNT, and GG–MWCNT. In the case of GG, some important peaks were presented at 2927, 1454, 1153 and 1021 cm^{-1} due to the C–H stretching, R–C–H asymmetric bending, C–O–C stretching, hydroxylic C–O single bond stretching of the C–O–C group in the anhydroglucose ring, respectively (Thakur, Chauhan, & Ahn, 2009). And the peak at 1560 cm^{-1} could be related to the C=C stretching of CNT (Hamon, Hui, Bhowmik, Itkis, & Haddon, 2002). In FTIR spectra of GG–MWCNT, the peak at 2897 cm^{-1} and the marked bands at 1059–1033 cm^{-1} were ascribed to C–H stretching and O–C stretching of GG, while the absorbance at 1570 cm^{-1} was indicative of MWCNT component. The new absorbance at 1727 cm^{-1} was characteristic of an ester (C=O stretching mode), which indicated the formation of covalent bonds between –OH groups of GG and MWCNT.

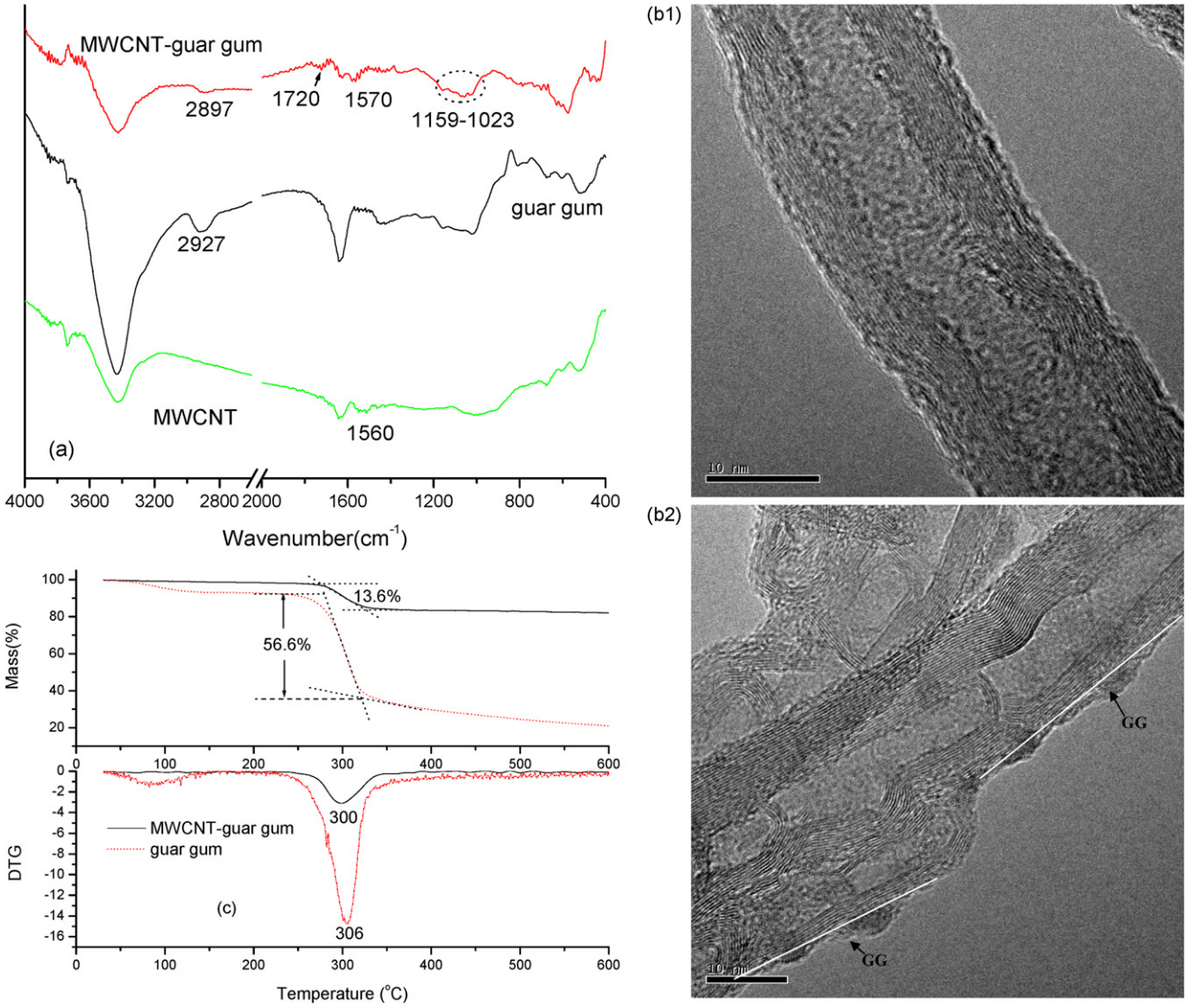

Fig. 1. (a) FTIR of spectra of GG, MWCNT, and GG–MWCNT, (b) TEM of MWCNT (b1) and GG–MWCNT (b2) and (c) the thermo gravimetric (TG) and derivative thermo gravimetric (DTG) curves of GG and GG–MWCNT.

As shown in Fig. 1b, the microstructures of MWCNT (b1) and GG–MWCNT (b2) were presented by TEM. Compared to MWCNT, the surface of GG–MWCNT was rough. It was clearly observed that MWCNT was wrapped by the grafted GG (as marked in Fig. 1b2) in GG–MWCNT composites.

Fig. 1c shows the thermogravimetric (TG) and derivative thermogravimetric (DTG) curves of GG and GG–MWCNT. The DTG curve revealed that the decomposed peak temperature of GG was exhibited at about 305 °C and the TG curve indicated the thermal decomposition of GG covered a range of temperature at maximum rate of mass loss. In the DTG curves, the decomposed peak temperature of GG was higher than GG in GG–MWCNT, which proved that GG had better thermal stability than GG in GG–MWCNT. It was reasonable to GG degradation during the synthesis of the GG–MWCNT. The GG–MWCNT displayed a mass loss of about 13.6 wt% at the range of GG decomposed temperature. It was assumed that the mass loss of GG at the decomposed temperature was still constant when GG grafted on MWCNT. The quantity of GG was calculated by matching mass loss (13.6 wt%) of GG–MWCNT to weight loss of GG (56.6 wt%) at the range of decomposed temperature. The GG content of GG–MWCNT was estimated to be about
24.0 wt%.

3.2. The dispersion of GG–MWCNT in aqueous solution

Fig. 2 shows the UV–vis spectra of MWCNT and GG–MWCNT in water at different concentrations, the featureless absorption in the 200–800 nm regions were similar to the spectra of MWCNT covalently functionalized by other polymers (Czerw, Guo, Ajayan, Sun, & Carroll, 2001; Lin, Rao, Sadanadan, Kenik, & Sun, 2002; Sun et al., 2001). In the spectra, the absorption peak at 265 nm was attributed to the characteristic absorption of MWCNT. The absorbance at 265 nm of MWCNT and GG–MWCNT depend on the solution concentrations in the linear fashion (Fig. 2a and b inset). The straight line passing through the origin described the relationship of the observed absorbance and MWCNT (or GG–MWCNT) concentrations. The linear correlation of GG–MWCNT ($R = 0.9998$) was higher than that of the MWCNT ($R = 0.9705$). It was obvious that GG–MWCNT in aqueous solution well followed the Lambert–Beer's

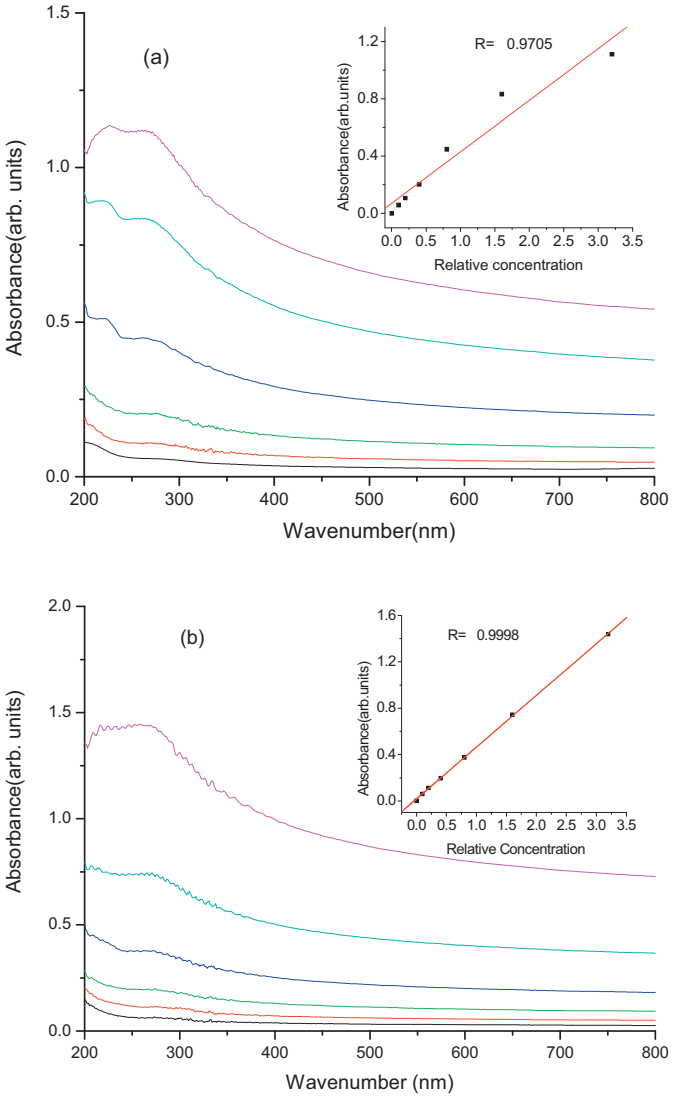

Fig. 2. UV–vis absorption spectra of MWCNT (a) and GG–MWCNT (b) in aqueous solutions. Inset: Lambert–Beer's plots for the absorption peak of MWCNT (a) and GG–MWCNT (b) at 265 nm.

law, because the GG component improved the hydrophobicity and the dispersion of MWCNTs in distilled water. In addition, sonications for the samples were performed and the intensity of absorption peak did not change. This indicated that the interaction between MWCNT and GG was not physical adsorption, but covalent grafting (Wu et al., 2007).

3.3. Characterization of GG–MWCNT–Fe_3O_4

As shown in Fig. 3a, iron oxide nanoparticles were evenly dispersed on the surface of GG–MWCNT without obvious aggregation. The size of iron oxide nanoparticles was about 5–10 nm. Polysaccharides present the dynamic supramolecular associations that are facilitated by inter- and intra-molecular hydrogen bonding, and can act as templates for nanoparticle growth (Yu, Yang, Liu, & Ma, 2009), preventing the nanoparticles from aggregating.

In Fig. 3b, there was a strong absorption peak at about 589 cm^{-1}, assigned to the characteristic absorption peak of Fe_3O_4 (Chang, Yu, Ma, & Anderson, 2011). And the components of GG and MWCNT were also observed in FTIR spectrum of GG–MWCNT–Fe_3O_4.

Fig. 3c shows the XRD patterns of GG–MWCNT–Fe_3O_4. The two peaks at about 25.8° and 42.9° corresponding to the structure of MWCNT also exist in the XRD pattern. The characteristic peaks of Fe_3O_4 were displayed at 2θ values of about 18.1°, 30.2°, 35.6°, 43.4°, 57.3° and 62.7° (Liu, Zhang, & Sasai, 2010), which illustrated that the magnetic Fe_3O_4 particles were successfully attached onto the surface of GG–MWCNT. This was also consistent with the TEM and FTIR results.

As revealed in Fig. 3d, the magnetization of GG–MWCNT–Fe_3O_4 as a function of the applied magnetic field at 298 K. Magnetization increased with an increasing magnetic field. The magnetization measurements showed the saturation magnetization of GG–MWCNT–Fe_3O_4 was 13.3 emu g^{-1} (magnetic field, ±10000 Oe).

3.4. Adsorption of the dyes

Fig. 4 illustrates the adsorption kinetics of cationic dyes by GG–MWCNT–Fe_3O_4 nanocomposite. The removal rates of dyes were very rapid during the initial stages of the adsorption processes. The instantaneous separation of GG–MWCNT–Fe_3O_4 from solution by exposing to a magnet could make sure to decrease the error of testing contact time. A large amount of MB or NR was rapidly removed by GG–MWCNT–Fe_3O_4 in the first 10 min, and then the rate of removal of dye slowed down gradually, finally the adsorption, respectively reached equilibrium values at 120 min for MB and at 20 min for NR. The adsorption kinetic process was described by the pseudo second-order model, expressed as Eq. (2) (Ofomaja, 2010):

$$\frac{t}{q_t} = \frac{1}{kq_e^2} + \frac{t}{q_e} \quad (2)$$

where k (g mg^{-1} min^{-1}) is the second-order rate constant, q_t (mg g^{-1}) and q_e (mg g^{-1}) represent the amount of dyes adsorbed at any time t (min) and at equilibrium, respectively. The second-order rate constant k and q_e can be calculated from the intercept and slope of the line in a t/q_t versus t. The kinetic parameters of dye adsorptions were shown in Table 1. For the adsorption of GG–MWCNT–Fe_3O_4, the linear relationship with high correlation coefficients ($R > 0.999$) between t/q_t and t indicated the adsorption process could be described well by the pseudo second-order model. In 1 L solution, the amounts of dye adsorbed at equilibrium were 37.17 mg MB and 28.36 mg NR by 1 g GG–MWCNT–Fe_3O_4, which were very close to the initial quantity of dye in the solution. It could be related to the hydrophilic property of GG, which improved the dispersion of GG–MWCNT–Fe_3O_4 in the solution, which facilitated the diffusion of dye molecules to the surface of CNTs (Gong et al., 2009).

As shown in Fig. 5a, the adsorption isotherm experiments for MB and NR were also carried out. The adsorption capacities, respectively reached 57.87 mg g^{-1} at MB equilibrium concentration of 9.5 mg L^{-1}, and 90.1 mg g^{-1} at NR equilibrium concentration of 83.3 mg L^{-1}. The experimental data could be analyzed by the

Table 1
The parameters of the adsorption of GG–MWCNT–Fe_3O_4 for MB and NR modeled by a pseudo second-order model and Langmuir model.

	Pseudo second-order model					Langmuir model		
	T_{eq} (min)	$q_{e,exp}$ (mg g^{-1})	$q_{e,cal}$ (mg g^{-1})	k (mg g^{-1} min^{-1})	R	q_m (mg g^{-1})	K_L (L mg^{-1})	R
MB	120	37.17	37.74	0.0067	1	61.92	0.87	0.998
NR	20	28.36	28.40	0.1293	1	89.85	0.39	0.994

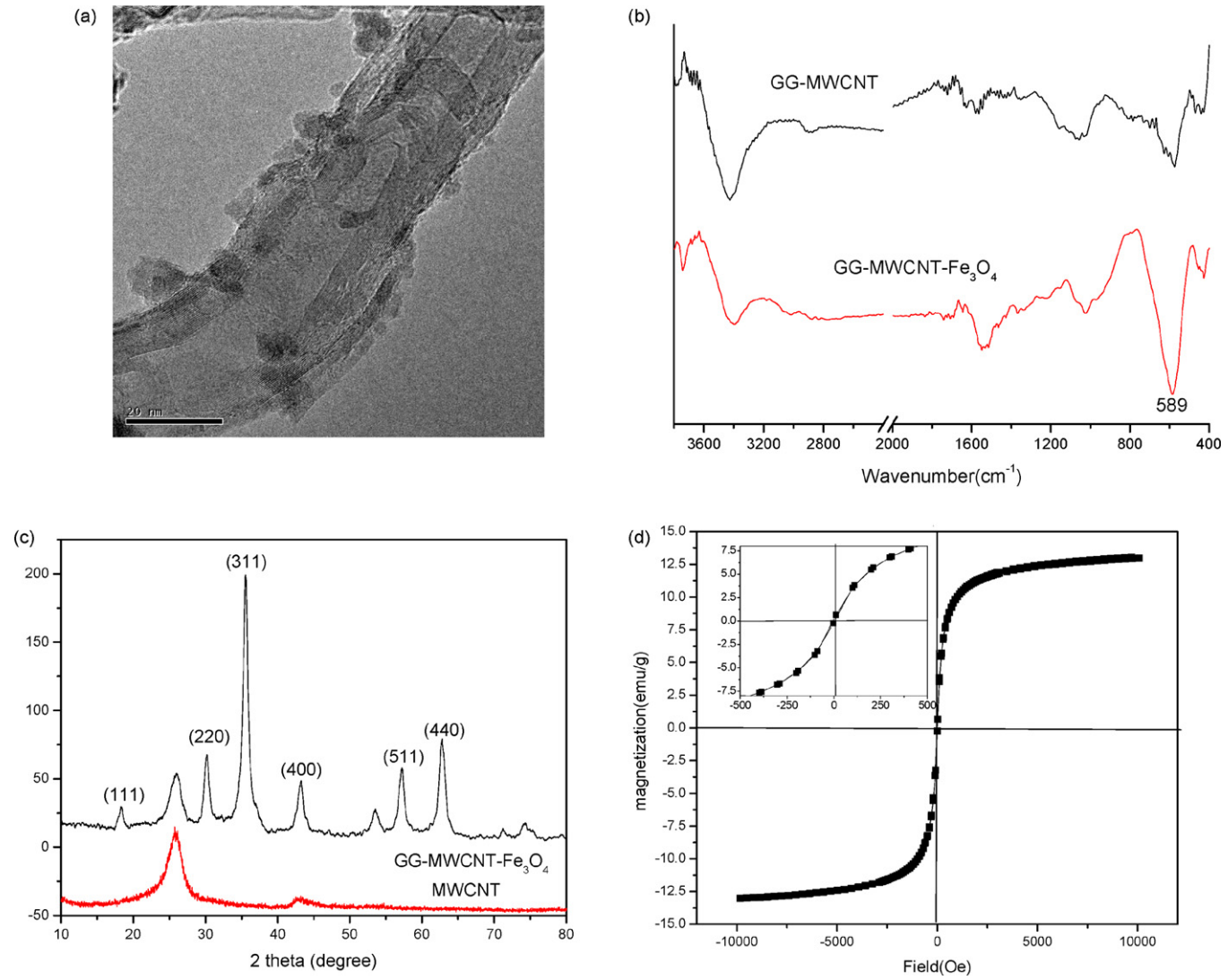

Fig. 3. (a) TEM of MWCNT–guar gum–Fe_3O_4, (b) FTIR of spectra of GG–MWCNT and GG–MWCNT–Fe_3O_4, (c) XRD patterns of GG–MWCNT–Fe_3O_4 and (d) The magnetic hysteresis loops of GG–MWCNT–Fe_3O_4. Inset: magnified view of the −500 to 500 Oe regions.

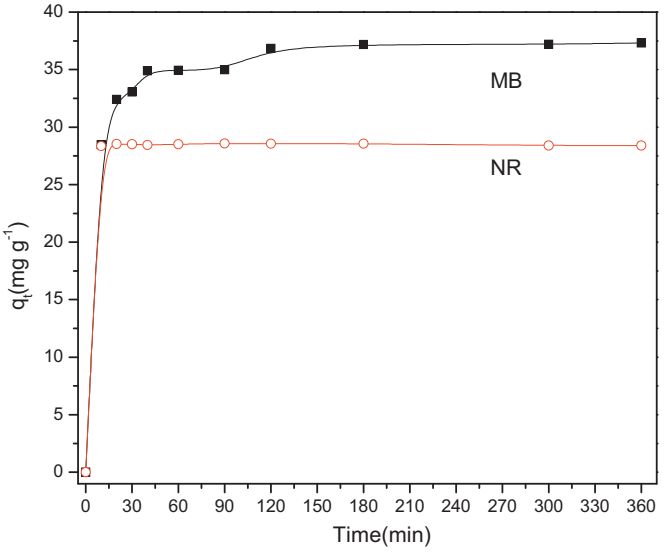

Fig. 4. The adsorption of GG–MWCNT–Fe_3O_4 for NR and MB; Initial concentration: MB, 0.1 mmol L^{-1} (37.4 mg L^{-1}); NR, 0.1 mmol L^{-1} (28.9 mg L^{-1}); GG–MWCNT–Fe_3O_4, 1 g L^{-1}.

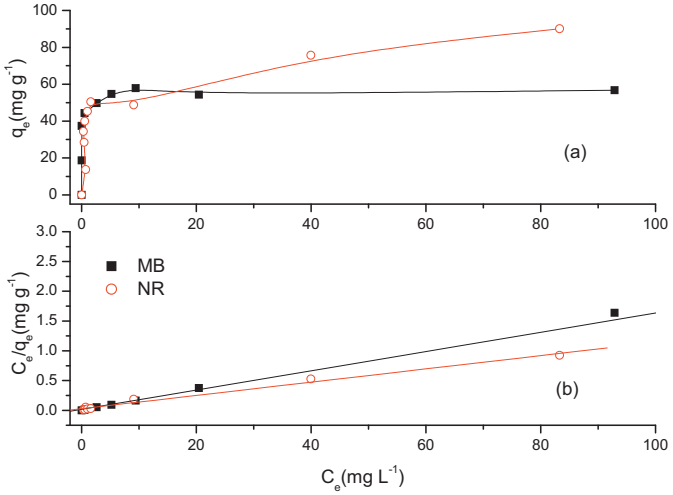

Fig. 5. (a) Adsorption isotherms of MB and NR by GG–MWCNT–Fe_3O_4 and (b) Langmuir isotherms for MB and NR by GG–MWCNT–Fe_3O_4. Initial concentration: MB 0.05–0.6 mmol L^{-1}, NR 0.05–0.6 mmol L^{-1}, GG–MWCNT–Fe_3O_4 1 g L^{-1}.

isotherm models of Langmuir, which assumed a surface with homogeneous binding sites, equivalent sorption energies, and no interaction between adsorbed species. Its mathematical form is written as Eq. (3) (Li et al., 2010):

$$q_e = \frac{q_m K_L C_e}{1 + K_L C_e} \quad (3)$$

where q_m and K_L are Langmuir constants related to maximum adsorption capacity and energy of adsorption, respectively. A straight line is obtained when C_e/q_e is plotted against C_e in Fig. 5b, and q_m and K_L could be calculated from the slopes and intercepts (Table 1). From the correlation coefficients ($R > 0.99$), the adsorption data fitted Langmuir isotherm model. The maximum adsorption of MB and NR reached 61.92 and 89.85 mg g^{-1}. The removal efficiency of cationic dyes using GG–MWCNT–Fe_3O_4 as adsorbents was compared with other adsorbents such as MWCNTs and MWCNT–Fe_3O_4 at 25 °C. It was found (Gong et al., 2009) that the q_m values for the adsorption of MB and NR by MWCNT–Fe_3O_4 were 15.87 and 20.51 mg g^{-1}. Yao, Xu, Chen, Xu, and Zhu (2010) reported that the q_m value was 46.2 mg g^{-1} for the adsorption of MB by CNTs. This phenomenon might be caused by the insignificant differences of CNT sources and experimental conditions. The comparison suggested that GG–MWCNT–Fe_3O_4 had great potential for use as dye adsorbents in wastewater treatment, and displayed the main advantage of separation convenience.

4. Conclusions

Guar gum was covalently grafted onto the surface of MWCNTs. GG (about 21.6 wt%) improved the dispersion of GG–MWCNT in water because of the hydrophilicity of GG. The UV absorbance was linearly dependent on the concentrations of GG–MWCNT in water, following Lambert–Beer's law. GG also assisted iron oxide nanoparticles to disperse on the MWCNT surface due to the supramolecular interaction between the metal ions and the hydroxyl groups of GG. The adsorption behavior of GG–MWCNT–Fe_3O_4 for MB and NR could be described well by the pseudo second-order model. The adsorption isotherm experiments revealed that the adsorption data fitted Langmuir isotherm model, and the maximum adsorption of GG–MWCNT–Fe_3O_4 for MB and NR reached 61.92 and 89.85 mg g^{-1}.

The magnetic GG–MWCNT–Fe_3O_4 possesses the properties of adsorption capacity and magnetic separation and can therefore be used as magnetic adsorbents to remove the contaminants from aqueous solutions.

Acknowledgement

Thanks for the supports from Nature Science Foundation of Jiangxi Province (No. 2010GZH0037) and National Nature Science Foundation of China (No. 51162011).

References

Bonnet, P., Albertini, D., Bizot, H., Bernard, A. & Chauvet, O. (2007). Amylose/SWNT composites: From solution to film—Synthesis, characterization and properties. *Composites Science and Technology*, *67*, 817–821.

Chang, P. R., Yu, J. G., Ma, X. F. & Anderson, D. P. (2011). Polysaccharides as stabilizers for the synthesis of magnetic nanoparticles. *Carbohydrate polymers*, *83*, 640–644.

Chatterjee, S., Chatterjee, T., Lim, S. R. & Woo, S. H. (2011). Effect of the addition mode of carbon nanotubes for the production of chitosan hydrogel core–shell beads on adsorption of Congo red from aqueous solution. *Bioresource Technology*, *102*, 4402–4409.

Crini, G. (2006). Non-conventional low-cost adsorbents for dye removal: A review. *Bioresource Technology*, *97*, 1061–1085.

Czerw, R., Guo, Z. X., Ajayan, P. M., Sun, Y. P. & Carroll, D. L. (2001). Organization of polymers onto carbon nanotubes: A route to nanoscale assembly. *Nano Letters*, *1*, 423–427.

Fu, C. L., Meng, L. J., Lu, Q. H., Zhang, X. K. & Gao, C. (2007). Large-scale production of homogeneous helical amylose/SWNTs complexes with good biocompatibility. *Macromolecular Rapid Communications*, *28*, 2180–2184.

Gong, J. L., Wang, B., Zeng, G. M., Yang, C. P., Niu, C. G., Niu, Q. Y., et al. (2009). Removal of cationic dyes from aqueous solution using magnetic multi-wall carbon nanotube nanocomposite as adsorbent. *Journal of Hazardous Materials*, *164*, 1517–1522.

Hamon, M. A., Hui, H., Bhowmik, P., Itkis, H. M. E. & Haddon, R. C. (2002). Ester- functionalized soluble single-walled carbon nanotubes. *Applied Physics A-Materials Science & Processing*, *74*, 333–338.

Ke, G. (2010). A novel strategy to functionalize carbon nanotubes with cellulose acetate using triazines as intermediated functional groups. *Carbohydrate Polymers*, *79*, 775–782.

Li, L., Meng, L. J., Zhang, X. K., Fu, C. L. & Lu, Q. H. (2009). The ionic liquid-associated synthesis of a cellulose/SWCNT complex and its remarkable biocompatibility. *Journal of Materials Chemistry*, *19*, 3612–3617.

Li, Y. H., Liu, F. Q., Xia, B., Du, Q. J., Zhang, P., Wang, D. C., et al. (2010). Removal of copper from aqueous solution by carbon nanotube/calcium alginate composites. *Journal of Hazardous Materials*, *177*, 876–880.

Lin, Y., Rao, A. M., Sadanadan, B., Kenik, E. A. & Sun, Y. P. (2002). Functionalizing multiple-walled carbon nanotubes with aminopolymers. *Journal of Physical Chemistry B*, *106*, 1294–1298.

Lin, Y., Taylor, S., Li, H. P., Shiral Fernando, K. A., Qu, L. W., Wang, W., et al. (2004). Advances toward bioapplications of carbon nanotubes. *Journal of Materials Chemistry*, *14*, 527–541.

Liu, Z. G., Zhang, F. S. & Sasai, R. (2010). Arsenate removal from water using Fe_3O_4-loaded activated carbon prepared from waste biomass. *Chemical Engineering Journal*, *160*, 57–62.

Long, R. Q. & Yang, R. T. (2001). Carbon nanotubes as superior sorbent for dioxins removal. *Journal of the American Chemical Society*, *123*, 2058–2059.

Ofomaja, A. E. (2010). Intraparticle diffusion process for lead (II) biosorption onto mansonia wood sawdust. *Bioresource Technology*, *101*, 5868–5876.

Sa, V. & Kornev, K. G. (2011). A method for wet spinning of alginate fibers with a high concentration of single-walled carbon nanotubes. *Carbon*, *49*, 1859–1868.

Sun, Y. P., Huang, W. J., Lin, Y., Fu, K. F., Kitaygorodskiy, A. & Riddle, L. A. (2001). Soluble dendron-functionalized carbon nanotubes: Preparation, characterization, and properties. *Chemistry of Materials*, *13*, 2864–2869.

Thakur, S., Chauhan, G. S. & Ahn, J. H. (2009). Synthesis of acryloyl guar gum and its hydrogel materials for use in the slow release of L-DOPA and L-tyrosine. *Carbohydrate Polymers*, *76*, 513–520.

Wang, J. P., Yang, H. C. & Hsieh, C. T. (2011). Adsorption of phenol and basic dye on carbon nanotubes/carbon fabric composites from aqueous solution. *Separation Science and Technology*, *46*, 340–348.

Wang, Y., Wei, F., Luo, G. H., Yu, H. & Gu, G. S. (2002). The large-scale production of carbon nanotubes in a nano-agglomerate fluidized-bed reactor. *Chemical Physics Letters*, *364*, 568–572.

Wu, Z. G., Feng, W., Feng, Y. Y., Liu, Q., Xu, X. H. & Sekino, T. (2007). Preparation and characterization of chitosan-grafted multiwalled carbon nanotubes and their electrochemical properties. *Carbon*, *45*, 1212–1218.

Xie, Y. F., Qian, D. Y., Wu, D. L. & Ma, X. F. (2011). Magnetic halloysite nanotubes/iron oxide composites for the adsorption of dyes. *Chemical Physics Letters*, *168*, 959–963.

Yan, L., Chang, P. R. & Zheng, P. W. (2011). Preparation and characterization of starch-grafted multiwall carbon nanotube composites. *Carbohydrate Polymers*, *84*, 1378–1383.

Yao, Y. J., Xu, F. F., Chen, M., Xu, Z. X. & Zhu, Z. W. (2010). Adsorption behavior of methylene blue on carbon nanotubes. *Bioresource Technology*, *101*, 3040–3046.

Yu, J. G., Yang, J. W., Liu, B. X. & Ma, X. F. (2009). Preparation and characterization of glycerol plasticized-pea starch/ZnO-carboxymethylcellulose sodium nanocomposites. *Bioresource Technology*, *100*, 2832–2841.